

Luminosity Optimisation by Adjusting LHC β^* at Collision.

W. Wittmer, CERN, Geneva, Switzerland and University of Technology Graz, Austria

Abstract

To correct the β^* at the main collision points (IP1 and IP5) simultaneously for the two counterrotating proton beams in the LHC a set of specific quadrupoles in the non-common part of the machine is used. Due to the antisymmetric optics, several quadrupoles on each side of the insertion have to be used. The change in the value of β^* is accomplished by changing the k values of the quadrupoles. This set of increments is referred to as β^* tuning knob. The increments were calculated by rematching β^* in a range of $\pm 20\%$ about the nominal value. Linear curves were fitted to the variation of increments to construct a linear tuning knob. This was done for each plane using MAD 8. The linear behaviour and the orthogonality of the knobs were investigated. Different field errors were introduced in the lattice and the correction efficiency of the knobs were studied.

1 INTRODUCTION

In operation during collision the beam sizes of the two beams have to be corrected. To do so, there have to be two orthogonal knobs to correct each plane independently. For these knobs a set of quadrupoles, which are located on each side of the IP in the insertion, are available. From these quadrupoles a knob is constructed so that a specific ΔK is assigned to each, which I refer to as knob vector, so that the β^* is changed. To scale the β^* the knob vector is multiplied with a variable K which is the actual knob. The knobs should have the following characteristics within a variation of $\pm 20\%$: be orthogonal in the x- and y- plane, create no betabeating in the rest of the ring, the scaling of the β^* with respect to the variable K be linear, no change of other constraints, be able to correct the β^* independently of the source of the error and be simple for operation.

The performance of the knobs have then to be tested. Therefore, both knobs, when varied over their nominal range, must meet the conditions of the different criteria described above. If this is the case the second stage of testing ist started. Various errors are introduced in the lattice and the knobs are used to correct them. This is done step by step to see to which types of errors the knobs can be applied.

2 CALCULATING β^* TUNING KNOBS

The design of the LHC insertion is asymmetric (see fig. 1) and the beams pass through the inner triplet (Q1-Q3 left and right from the IP) in a common beam pipe offcenter of

the magnetic field axis. Therefore the magnets of the inner triplet cannot be used to adjust the β^* .

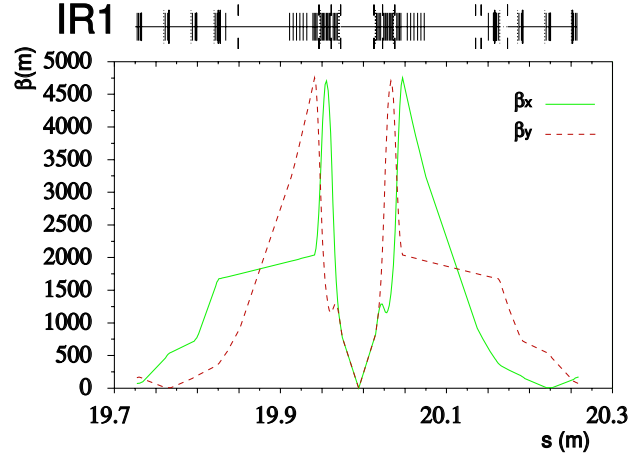


Figure 1: β -functions at IR1 between Q7 left and right from IP1.

The closest magnet that can be used is Q4 left and right of the IP. There are further three quadrupoles (Q5-Q7) which can be used without any restriction. Because of the asymmetric β -functions, the different phase advance and the need to correct both planes, there is no pair of quadrupoles that can do the correction for either of the planes without changing the other plane's β -function. The position of the different tuning quadrupoles and the dipoles separating and combining the two beams are shown in fig.2.

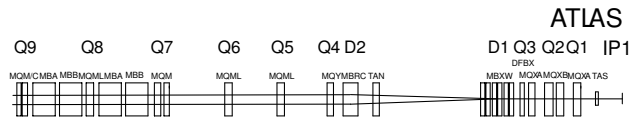


Figure 2: Position of the different magnets in IR1 and parts of the dispersion suppressor.

With the chosen qadrupoles the knob vector is calculated using MAD8. The version of the lattice file for the LHC is collision optics V6.2.

The first knob vector was constructed using Q4 to Q7 left and right from IP1. As constraints where chosen β^* , α^* and two β -functions values at two points in the ring outside the insertion which are seperated by a phase advance of $\phi = \frac{\pi}{4}$. This was done for both planes. The β^* -value of one plane is set to the nominal value, for the LHC at collision equal to 0.5 meters, so as to create no change of the β -function

in this plane, while the other is varied to create the desired change. The β^* is matched in small steps and the resulting ΔK of the tuning quadrupoles are shown in fig.3 as a function of β^* . Both α^* values are set to their nominal values to keep the beam waist of both planes at the IP. To suppress a β beating (change of the β -function around the whole ring) is the aim of the last four constraints. Fitting linear curves to the plot shown in fig.3 yielded a knob vector which only worked for a specific value of ΔK and a narrow region around it. With greater distance to this value, the constraints changed. The variation of the fitted curves only moved the optimized ΔK value without improving the knob vector as a whole. Different new knob vectors with different sets of constraints and variation of the fitted curves were calculated, but all gave the same result.

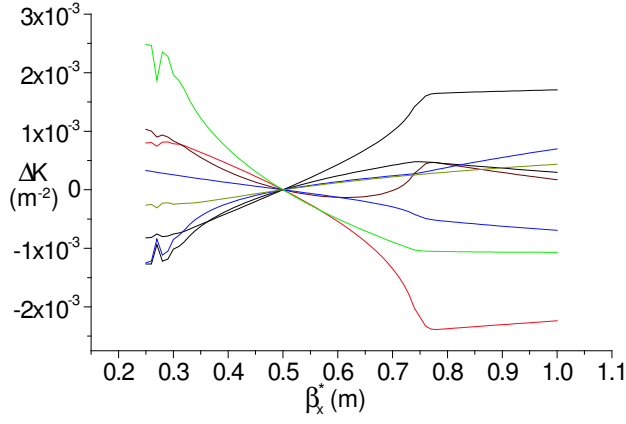


Figure 3: The change of the tuning quadrupoles as a function of β^* , $\Delta K = f(\beta_x^*)[m^{-2}]$, which are obtained by match. The chosen constraints are $\beta_x^*, \beta_y^*, \alpha_x^*, \alpha_y^*$ at IP1 and β_x, β_y at the quadrupole slices **MQY.A4R8.B1..1** and **MQY.A4L8.B1..2**, which have a phase advance of $\Delta\phi \approx \frac{\pi}{2}$.

Because of this, the lattice was analyzed to extend the number of tuning quadrupoles on both sides of the IP. There are further two quadrupoles on each side (Q8 and Q9) which are part of the dispersion suppressor. To use these means to create additional dispersion at the IP beside the one introduced by the crossing angle. By changing K of Q13 with the same relative change as Q9 the introduced dispersion can be reduced. This additional dispersion must not be greater than the one from the crossing angle and the one created by the error to be corrected. The additional dispersion, if too big, increases the beam size. For the LHC the nominal beam size at collision is $14\mu m$. With the nominal energie spread $\delta_e = 1.10 \cdot 10^{-4}$ the dispersion must be smaller than $D \leq 1 \cdot 10^{-2}[m]$ according to the relation $\sigma = \sqrt{(\beta \cdot \epsilon) + (D \cdot \delta_e)^2}$. The relation between β and ΔK for the tuning quadrupoles are plotted in Fig.4.

In first approximation the curves are linear. The tuning knob vectors created with linear fits show for a variation of β^* by $(+100/-25)\%$ a much improved better behaviour.

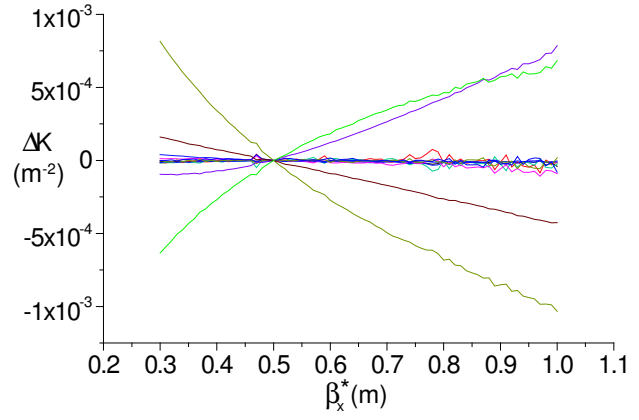


Figure 4: The change of the tuning quadrupoles as a function of β^* , $\Delta K = f(\beta_x^*)[m^{-2}]$, which are obtained by match. The chosen constraints are $\beta_x^*, \beta_y^*, \alpha_x^*, \alpha_y^*$ at IP1 and β_x, β_y at the quadrupole slices **MQY.A4R8.B1..1** and **MQY.A4L8.B1..2**, which have a phaseadvance of $\Delta\phi \approx \frac{\pi}{2}$.

After all the usable intervall of $\pm 20\%$ is much smaller and therefore enough safety margin remains. As one can see in fig. 4 four tuning quadrupoles change more than the other eight which seem to fluctuate around the zero line. We tried to only use these four for matching, but it did not lead to reasonable results. The machted β_x^* value does only change about $(+0.02/-0.1)[m]$ although it should change $(+0.5/-0.25)[m]$. Additionally to this β_y^* is changed by $\approx -20\%$. Even as the functions $\Delta K = f(\beta_x^*)$ are linear, as shown in fig.5, a linear scaling implies a far to big change of the constraints, which are to be keep constant. Also a scaling of ΔK would exceed the limits of maximum powering of the quadrupoles.

The variation of $\Delta\beta_x^*, \Delta\beta_y^*, \Delta\alpha_x^*, \Delta\alpha_y^*, Q_x, Q_y, D_x, Dp_x$ as a function of $\Delta\beta_x^*$ and $\Delta\beta_y^*$ is documented in the plots Fig.12, 5 - Fig.19, 6. In these cases the knobs were applied simultaneously. The ranges of the x - and y - axes are $(-50/+100)\%$. The results for the variation of $\pm 20\%$ are summarized in table1.

Table 1: Changes of $\Delta\beta_x^*, \Delta\beta_y^*, \Delta\alpha_x^*, \Delta\alpha_y^*, Q_x, Q_y, D_x, Dp_x$ as a function of $\Delta\beta_x^*$ and $\Delta\beta_y^*$ for $\pm 20\%$ changes.

VAR	β_x^*	+20%	+20%	-20%	-20%
	β_y^*	+20%	-20%	+20%	-20%
$\Delta\beta_x^*/[\%]$		-0.72	0.69	0.41	-0.44
$\Delta\beta_y^*/[\%]$		-0.47	0.44	0.38	-0.42
$\Delta\alpha_x^*/[1]$		0.023	0.019	0.017	0.023
$\Delta\alpha_y^*/[1]$		-0.027	-0.013	-0.016	-0.029
$\Delta Q_x/[1]$		0.0083	0.0046	-0.0069	-0.0098
$\Delta Q_y/[1]$		0.0049	-0.0104	0.0071	-0.0052
$\Delta D_x^*/[m]$		0.010	0.0069	-0.0060	-0.0084
$\Delta Dp_x^*/[1]$		-0.0073	-0.0040	0.0023	0.0031

The changes of $\Delta\beta_x^*, \Delta\beta_y^*, \Delta\alpha_x^*, \Delta\alpha_y^*, \Delta Q_x$ and ΔQ_y are acceptable for adjustments in operations. The dispersion

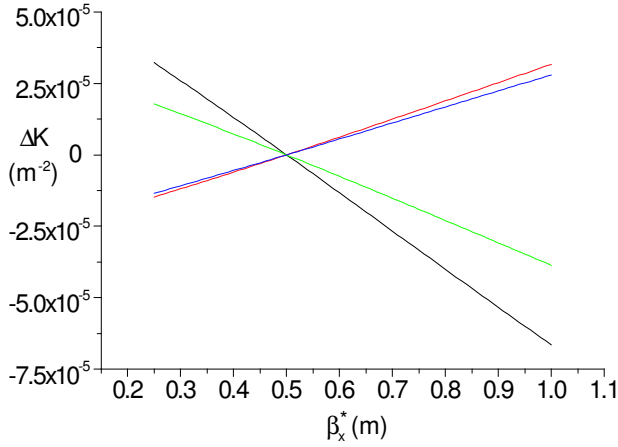


Figure 5: The changes of the tuning quadrupoles **KQ8.L1B1**, **KQ7.R1B1** - **KQ9.R1B1** and **KQ13.R1B1** as a function of β_x^* , $\Delta K = f(\beta_x^*)[m^{-2}]$, which are obtained by match. The chosen constraints are β_x^* , β_y^* , α_x^* , α_y^* at IP1 and β_x , β_y at the quadrupole slices **MQY.A4R8.B1..1** and **MQY.A4L8.B1..2**, which have a phase advance of $\Delta\phi \approx \frac{\pi}{2}$. The values at the x -axis are the matching goals which are failed by a factor ≈ 100 .

reaches the threshold for a change of (+20/ +20)%. This has to be investigated closer.

The orthogonality behaviour ($\Delta\beta_x^* = f(\beta_x^*, \beta_x^*)$, $\Delta\beta_y^* = f(\beta_x^*, \beta_x^*)$), as shown in plot 12, 5 and plot 13 5 of both knobs is different. The reason for this is the asymmetric lattice as mentioned before. Due to other reasons, the lattice is not strictly asymmetric. This can be seen in the values for the β -functions which are shown in Table 2.

Table 2: Relation of the β -functions at IR1.

NAME	β_x	β_y	$\frac{\beta_x}{\beta_y}$	$\frac{\beta_y}{\beta_x}$
KQ13.L1B1	30.9987	175.199		5.65182
KQ9.L1B1	13.3884	163.777		12.2328
KQ8.L1B1	141.876	10.5264	13.4781	
KQ7.L1B1	76.4196	167.610		2.19329
KQ6.L1B1	515.796	6.69436	77.0493	
KQ5.L1B1	745.398	180.832	4.12205	
KQ4.L1B1	1648.63	363.751	4.53230	
IP1	0.50000	0.50000	1.0	
KQ4.R1B1	363.751	1648.63		4.53230
KQ5.R1B1	180.832	745.398		4.12204
KQ6.R1B1	6.69436	515.796		77.0493
KQ7.R1B1	167.927	76.2554	2.20217	
KQ8.R1B1	12.2194	133.042		10.8878
KQ9.R1B1	132.846	37.8208	3.51251	
KQ13.R1B1	172.108	34.3219	5.01452	

The first column shows the name of the tuning quadrupoles, columns two and three the β -functions taken at the center of the quadrupoles and columns four and five the ratios $\frac{\beta_x}{\beta_y}$ and $\frac{\beta_y}{\beta_x}$. Only values greater than one for the ratios are shown

to indicate which β exactly is greater than the other. Also the phase advance is not antisymmetric around the IP as shown in Table 3.

Table 3: Phaseadvance $\Delta\mu$ between the tuning quadrupoles and IP1.

NAME	$\Delta\mu_x$	$\Delta\mu_y$
KQ9.L1B1	0.5370	1.0764
KQ8.L1B1	0.3661	0.8894
KQ7.L1B1	0.2996	0.7063
KQ6.L1B1	0.2708	0.4787
KQ5.L1B1	0.2623	0.2804
KQ4.L1B1	0.2584	0.2637
KQ4.R1B1	0.2637	0.2584
KQ5.R1B1	0.2804	0.2623
KQ6.R1B1	0.4787	0.2708
KQ7.R1B1	0.7063	0.2996
KQ8.R1B1	0.8654	0.3679
KQ9.R1B1	1.0778	0.4723

All this contributes to the different behaviour of the planes because a change of the β -function at the IP is related to these variables as follows:

$$\Delta\beta^* = \frac{\beta^*}{2 \sin(2\pi Q)} \oint \beta(s) \Delta K(s) \cos(2|\Delta\mu| - 2\pi Q) ds$$

In addition the dispersion ΔD_x and β functions have to be observed around the ring. A change in either of these functions will cause a change of the parameters at other IP's which should be avoided. The β function in the x - plane is shown in fig.6. There is no change except in the region of IP1, due to the variation of the tuning quadrupoles around IP1.

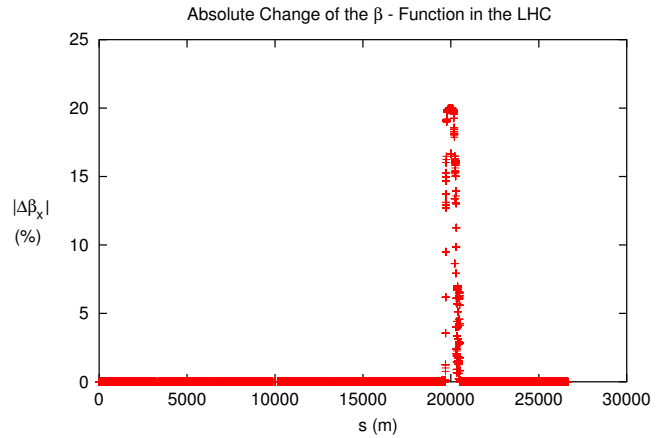


Figure 6: Change of the β function in the x - plane when the IP1 tuning knob for this plane is applied. The changes occur only in the region between **KQ13.L1B1** and **KQ13.R1B1**.

A zoom of this region is shown in fig.7, 4. The betafunction at IP1 is changed to the matched value. Fig.8 shows the same situation for the y - plane. Here the β function only changed in the region of the tuning quadrupoles to keep it

constant at the IP. This proves the orthogonal behaviour of the knobs.

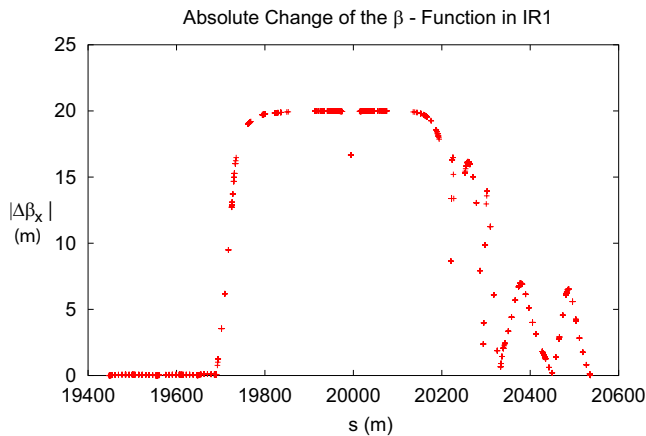


Figure 7: Change of the β function between **KQ13.L1B1** and **KQ13.R1B1** in the x - plane when the tuning knob for this plane is applied. In order to have the wanted change at the IP the incoming β function creates this change. The outgoing betafunction has to be changed to have no β beating in the ring.

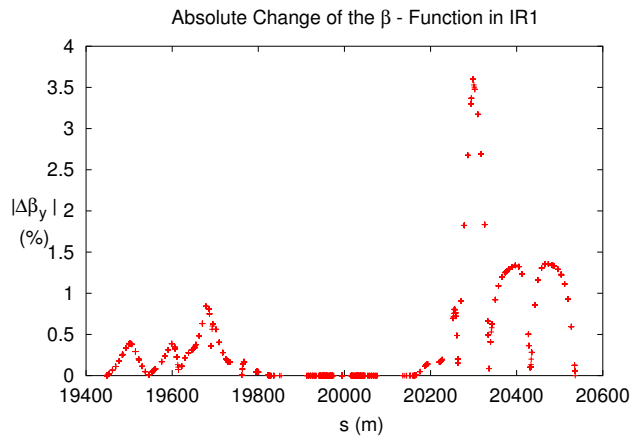


Figure 8: Change of the β function between **KQ13.L1B1** and **KQ13.R1B1** in the y - plane when the tuning knob for the other plane is applied. This shows the orthogonal behaviour of this knob.

For the dispersion the situation is simpler. As there is only the x - plane to be observed there is no cross talk of the planes. Fig.9 shows the dispersion function around the ring. There are changes of approx. $0.05[m]$ in most of the ring with some exceptions with approx. $0.1[m]$. The biggest changes are in IR1 and IR5. Fig. 10 presents a zoom of the IP1 region.

So far the results are acceptable. Further studies of different combinations of constraints will show if further improvement of the behavior can be obtained.

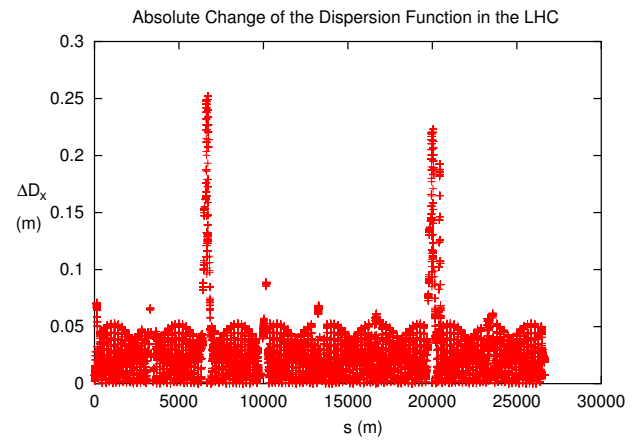


Figure 9: Dispersion beat around the ring created by applying the tuning knob for the x - plane. The biggest changes of the dispersion are in IR1 and IR5.

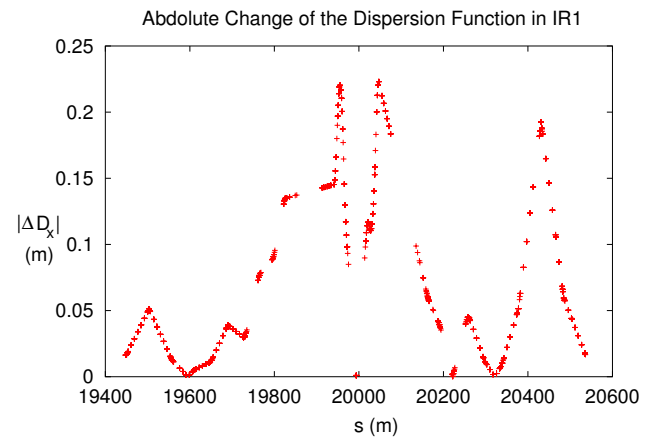


Figure 10: Zoom of figure 9 showing the region between **KQ13.L1B1** and **KQ13.R1B1**. The change of the dispersion at the IP is smaller than in the rest of the region.

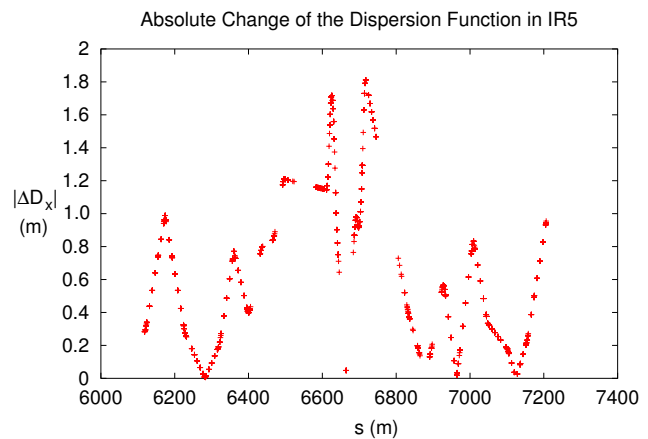


Figure 11: Zoom of figure 9 showing the region between **KQ13.L5B1** and **KQ13.R5B1**. The change of the dispersion at the IP is smaller than in the rest of the region.

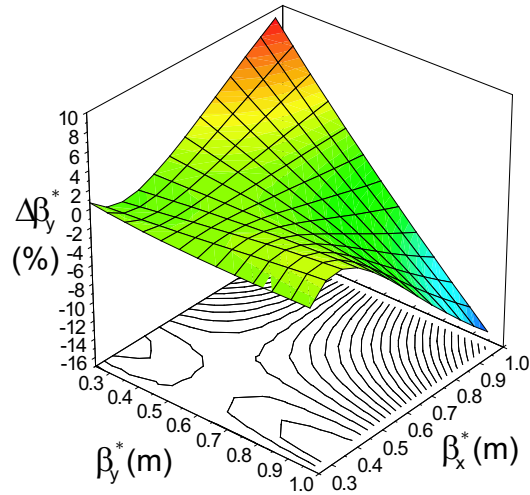


Figure 12: Orthogonality behaviour of the β_x^* knob. $\Delta\beta_y^*$ is shown as a function of β_x^* and β_y^* ($\Delta\beta_y^* = f(\beta_x^*, \beta_y^*)$). To only see the change of β_y^* created by the β_x^* knob, $\Delta\beta_y^*$ is normalized as following: $\Delta\beta_y^* = \frac{\beta_{y_{ist}}^* - \beta_{y_{soll}}^*}{\beta_{y_{soll}}^*}$. $\beta_{y_{ist}}^*$ is the actual value and $\beta_{y_{soll}}^*$ is the value if only the knob vector for β_y^* is applied. The ranges on the x - and y - axes are (+100/ - 50)%.

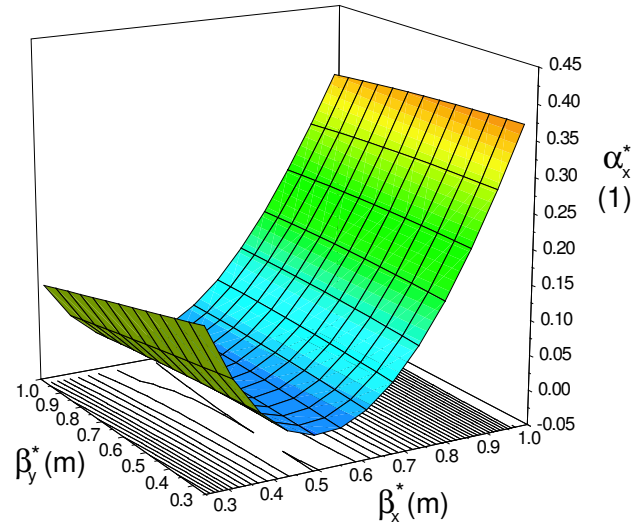


Figure 14: Influence of the knob vectors on the horizontal α -function at IP1 $\alpha_x^* = f(\beta_x^*, \beta_y^*)$. On the x - and y - axes the values of the β -functions at IP1 for both planes, β_x^* and β_y^* , are shown within a range of (+100/ - 50)%. On the z - axis α_x^* is shown.

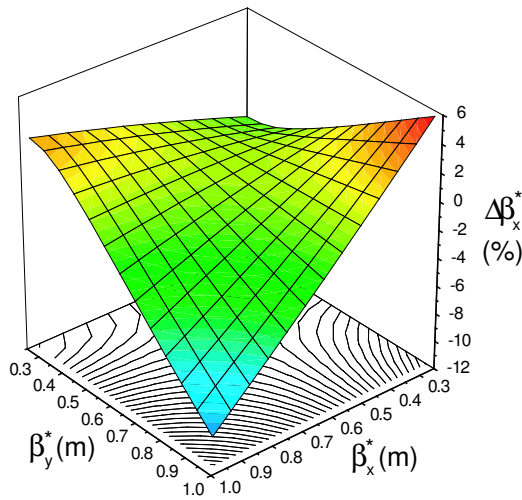


Figure 13: Orthogonality behaviour of the β_y^* knob. $\Delta\beta_x^*$ is shown as a function of β_x^* and β_y^* ($\Delta\beta_x^* = f(\beta_x^*, \beta_y^*)$). To only see the change of β_x^* created by the β_y^* knob, $\Delta\beta_x^*$ is normalized as following: $\Delta\beta_x^* = \frac{\beta_{x_{ist}}^* - \beta_{x_{soll}}^*}{\beta_{x_{soll}}^*}$. $\beta_{x_{ist}}^*$ is the actual value and $\beta_{x_{soll}}^*$ is the value if only the knob vector for β_x^* is applied. The ranges on the x - and y - axes are (+100/ - 50)%.

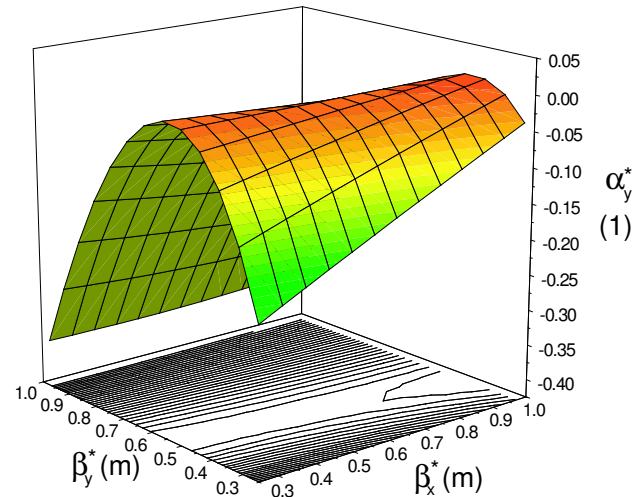


Figure 15: Influence of the knob vectors on the vertical α -function at IP1 $\alpha_y^* = f(\beta_x^*, \beta_y^*)$. On the x - and y - axes the values of the β -functions at IP1 for both planes, β_x^* and β_y^* , are shown within a range of (+100/ - 50)%. On the z - axis α_y^* is shown.

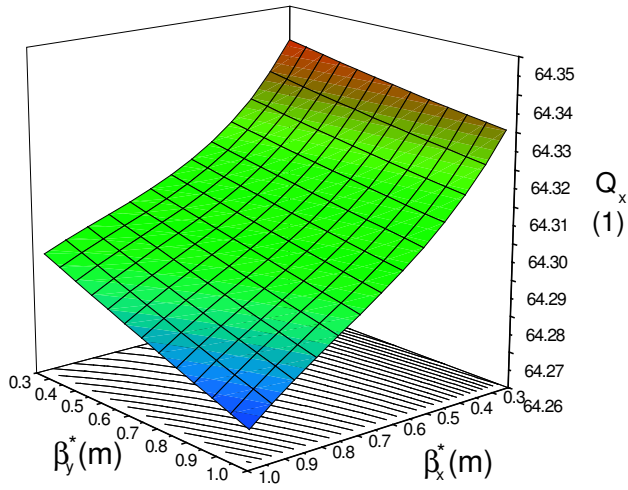


Figure 16: Influence of the knob vectors on the horizontal tune $Q_x = f(\beta_x^*, \beta_y^*)$. On the x - and y - axes the values of the β -functions at IP1 for both planes, β_x^* and β_y^* , are shown within a range of (+100/ - 50)%. On the z - axis Q_x is shown.

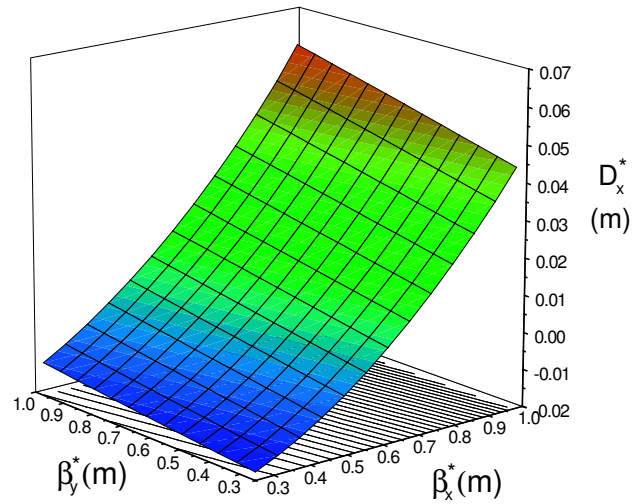


Figure 18: Influence of the knob vectors on the dispersion $D_x = f(\beta_x^*, \beta_y^*)$ at IP1. On the x - and y - axes the values of the β -functions at IP1 for both planes, β_x^* and β_y^* , are shown within a range of (+100/ - 50)%. On the z - axis D_x is shown.

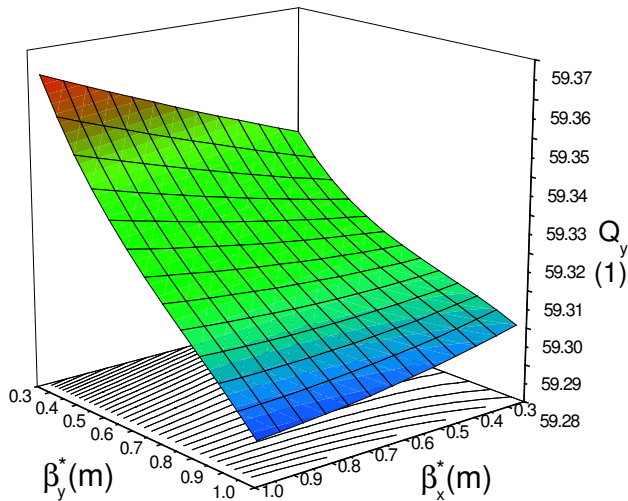


Figure 17: Influence of the knob vectors on the vertical tune $Q_y = f(\beta_x^*, \beta_y^*)$. On the x - and y - axes the values of the β -functions at IP1 for both planes, β_x^* and β_y^* , are shown within a range of (+100/ - 50)%. On the z - axis Q_y is shown.

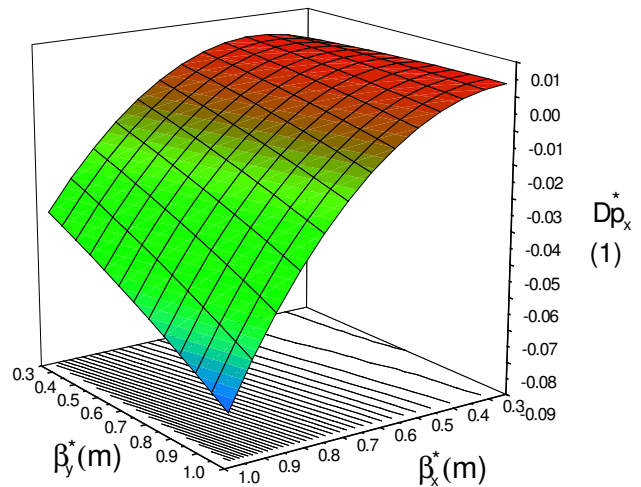


Figure 19: Influence of the knob vectors on the change of the dispersion $Dp_x = f(\beta_x^*, \beta_y^*)$ at IP1. On the x - and y - axes the values of the β -functions at IP1 for both planes, β_x^* and β_y^* , are shown within a range of (+100/ - 50)%. On the z - axis Dp_x is shown.

3 TESTS

To test the behaviour of the knobs errors are introduced into the lattice. A preliminary correction is applied, e.g., orbit correction for $B1$ field errors, and $B3, B4, B5, A2, A3$ correction, based on magnetic field measurements. Then the tuning knobs were applied and their effect was observed. To obtain a diversified result demonstrating for which type of error the knobs work a test program as shown in Fig.20 is followed.

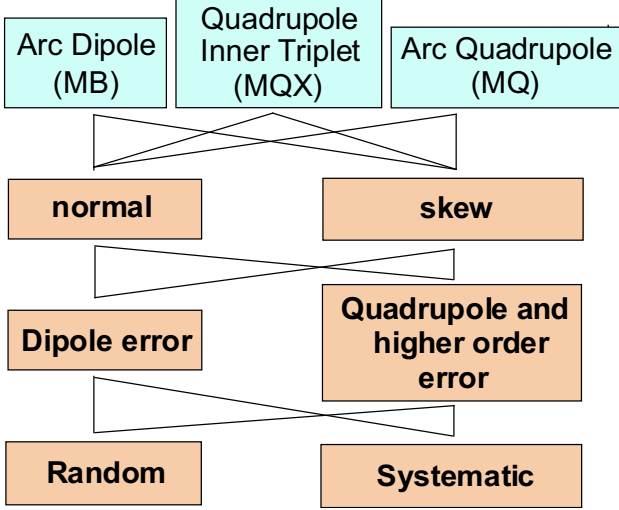


Figure 20: Description of the testprogram.

So far errors were introduced in arc dipoles **MB** and arc quadrupoles **MQ**. As error field types **B1** to **B11** have been applied. For all different cases the β^* values at IP1 could be corrected. A summary of the results for the case, when errors in all the magnets with all field error types were introduced in the lattice described above, is shown in Table 4.

Table 4: Results from the test run with systematic and random errors of the field type **B1** to **B11** in the arc dipoles **MB** and arc quadrupoles **MQ**.

	mean value	rms	min	max
$\Delta\beta_x$	2.1E-02	1.5E-02	-1.1E-03	-6.9E-02
$\Delta\beta_y$	2.3E-02	1.8E-02	1.2E-03	8.6E-02
ΔD_x	1.4E-02	5.1E-02	-1.5E-04	-3.9E-01
ΔDp_x	4.0E-02	1.9E-01	3.8E-04	-1.5E+00
ΔQ_x	7.2E-02	4.6E-02	-3.2E-03	1.8E-01
ΔQ_y	5.6E-02	3.5E-02	3.0E-04	-1.3E-01
	tk appl	tk appl		
$\Delta\beta_x$	5.0E-01	5.0E-01		
$\Delta\beta_y$	5.0E-01	5.0E-01		
ΔD_x	1.5E-03	-1.6E-02		
ΔDp_x	-8.9E-03	-3.2E-02		
ΔQ_x	64.313	64.312		
ΔQ_y	59.322	59.317		

Columns two and three show the mean value and rms of the

changes between the introduction of the errors and the application of the tuning knobs, column four the minimum, column five the maximum change out of sixty different seeds and columns six and seven the resulting final values of $\beta_x, \beta_y, D_x, D_y, Q_x, Q_y$ for the same seed as for the maximum and minimal change after the tuning knobs were applied.

4 CONCLUSION

So far the characteristics of the calculated tuning knobs are within the given boundaries. Normal field error types in the arc dipoles and quadrupoles can be corrected with these knobs. The change of the dispersion in IP1, when applying the tuning knobs, has to be followed up. The skew field errors and errors in the inner triplet quadrupoles have to be tested to determine the applicability of the knobs for these cases. The action of the knobs in presence of a closed orbit distortion will also be investigated. Finally beam beam effects and the reaction of the knobs to these will complement the picture of the behaviour of the knobs.

The results show, that even in complicated designs as for the LHC tuning procedures can be developed. Following a similar scheme as described above, IP β -function tuning knobs could also be computed for linear colliders, such as CLIC.

5 ACKNOWLEDGEMENT

I thank A. Verdier, M. Hayes and F. Zimmermann for comments and informations.

6 REFERENCES

- [1] H. Grote and F. C. Iselin, "The MAD program (methodical accelerator design) version 8.4: User's reference manual," CERN-SL-90-13-AP-REV.2.
- [2] N.J. Walker, J. Irwin, M. Woodley, "GLOBAL TUNING KNOBS FOR THE SLC FINAL FOCUS." SLAC-PUB-6207, Apr 1993. 3pp. Presented at 1993 Particle Accelerator Conference (PAC 93), Washington, DC, 17-20 May 1993. In *Washington 1993, Particle accelerator* 95-97.
- [3] Y. Nosochkov, P. Raimondi, T.O. Raubenheimer, A. Seryi, M. Woodley "TUNING KNOBS FOR THE NLC FINAL FOCUS." SLAC-PUB-9255, Jun 2002. 4pp. Presented at 8th European Particle Accelerator Conference (EPAC 2002), Paris, France, 3-7 Jun 2002. e-Print Archive: physics/0206068